EUROPEAN ORGANISATION FOR NUCLEAR RESEARCH

CERN-PPE/91-91
11 June 1991

A Direct Observation of Quark-Gluon Jet Differences at LEP

The OPAL Collaboration

Abstract

Quark and gluon jets in e^+e^- 3-jet events at LEP are identified using lepton tagging of quark jets, through observation of semi-leptonic charm and bottom quark decays. Events with a symmetry under transposition of the energies and directions of a quark and gluon jet are selected: these quark and gluon jets have essentially the same energy and event environment and as a consequence their properties can be compared directly. The energy of the jets which are studied is about 24.5 GeV. In the cores of the jets, gluon jets are found to yield a softer particle energy spectrum than quark jets. Gluon jets are observed to be broader than quark jets, as seen from the shape of their particle momentum spectra both in and out of the 3-jet event plane. The greater width of gluon jets relative to quark jets is also visible from the shapes of their multiplicity distributions. Little difference is observed, however, between the mean value of particle multiplicity for the two jet types.

(Submitted to Physics Letters B)

The OPAL Collaboration

G. Alexander[23], J. Allison[16], P.P. Allport[5], K.J. Anderson[9], S. Arcelli[2], J.C. Armitage[6], P. Ashton[16], A. Astbury[a], D. Axen[b], G. Azuelos[18,c], G.A. Bahan[16], J.T.M. Baines[16], A.H. Ball[17], J. Banks[16], G.J. Barker[13], R.J. Barlow[16], J.R. Batley[5], G. Beaudoin[18], A. Beck[23], J. Becker[10], T. Behnke[8], K.W. Bell[20], G. Bella[23], S. Bethke[11], O. Biebel[3], U. Binder[10], I.J. Bloodworth[1], P. Bock[11], H.M. Bosch[11], S. Bougerolle[b], B.B. Brabson[12], H. Breuker[8], R.M. Brown[20], R. Brun[8], A. Buijs[8], H.J. Burckhart[8], P. Capiluppi[2], R.K. Carnegie[6], A.A. Carter[13], J.R. Carter[5], C.Y. Chang[17], D.G. Charlton[8], J.T.M. Chrin[16], P.E.L. Clarke[25], I. Cohen[23], W.J. Collins[5], J.E. Conboy[15], M. Cooper[22], M. Couch[1], M. Coupland[14], M. Cuffiani[2], S. Dado[22], G.M. Dallavalle[2], S. De Jong[8], P. Debu[21], M.M. Deninno[2], A. Dieckmann[11], M. Dittmar[4], M.S. Dixit[7], E. Duchovni[26], G. Duckeck[11], I.P. Duerdoth[16], D.J.P. Dumas[6], G. Eckerlin[11], P.A. Elcombe[5], P.G. Estabrooks[6], E. Etzion[23], F. Fabbri[2], M. Fincke-Keeler[a], H.M. Fischer[3], D.G. Fong[17], C. Fukunaga[24], A. Gaidot[21], O. Ganel[26], J.W. Gary[11], J. Gascon[18], R.F. McGowan[16], N.I. Geddes[20], C. Geich-Gimbel[3], S.W. Gensler[9], F.X. Gentit[21], G. Giacomelli[2], V. Gibson[5], W.R. Gibson[13], J.D. Gillies[20], J. Goldberg[22], M.J. Goodrick[5], W. Gorn[4], C. Grandi[2], E. Gross[26], J. Hagemann[8], G.G. Hanson[12], M. Hansroul[8], C.K. Hargrove[7], P.F. Harrison[13], J. Hart[5], P.M. Hattersley[1], M. Hauschild[8], C.M. Hawkes[8], E. Heflin[4], R.J. Hemingway[6], R.D. Heuer[8], J.C. Hill[5], S.J. Hillier[1], D.A. Hinshaw[18], C. Ho[4], J.D. Hobbs[9], P.R. Hobson[25], D. Hochman[26], B. Holl[8], R.J. Homer[1], S.R. Hou[17], C.P. Howarth[15], R.E. Hughes-Jones[16], R. Humbert[10], P. Igo-Kemenes[11], H. Ihssen[11], D.C. Imrie[25], L. Janissen[6], A. Jawahery[17], P.W. Jeffreys[20], H. Jeremie[18], M. Jimack[2], M. Jobes[1], R.W.L. Jones[13], P. Jovanovic[1], D. Karlen[6], K. Kawagoe[24], T. Kawamoto[24], R.K. Keeler[a], R.G. Kellogg[17], B.W. Kennedy[15], C. Kleinwort[8], D.E. Klem[19], T. Kobayashi[24], T.P. Kokott[3], S. Komamiya[24], L. Köpke[8], R. Kowalewski[6], H. Kreutzmann[3], J. von Krogh[11], J. Kroll[9], M. Kuwano[24], P. Kyberd[13], G.D. Lafferty[16], F. Lamarche[18], W.J. Larson[4], J.G. Layter[4], P. Le Du[21], P. Leblanc[18], A.M. Lee[17], M.H. Lehto[15], D. Lellouch[8], P. Lennert[11], C. Leroy[18], L. Lessard[18], S. Levegrün[3], L. Levinson[26], S.L. Lloyd[13], F.K. Loebinger[16], J.M. Lorah[17], B. Lorazo[18], M.J. Losty[7], X.C. Lou[12], J. Ludwig[10], M. Mannelli[8], S. Marcellini[2], G. Maringer[3], A.J. Martin[13], J.P. Martin[18], T. Mashimo[24], P. Mättig[3], U. Maur[3], T.J. McMahon[1], J.R. McNutt[25], F. Meijers[8], D. Menszner[11], F.S. Merritt[9], H. Mes[7], A. Michelini[8], R.P. Middleton[20], G. Mikenberg[26], J. Mildenberger[6], D.J. Miller[15], C. Milstene[23], R. Mir[12], W. Mohr[10], C. Moisan[18],

A. Montanari[2], T. Mori[24], M.W. Moss[16], T. Mouthuy[12], P.G. Murphy[16], B. Nellen[3], H.H. Nguyen[9], M. Nozaki[24], S.W. O'Neale[8,d], B.P. O'Neill[4], F.G. Oakham[7], F. Odorici[2], M. Ogg[6], H.O. Ogren[12], H. Oh[4], C.J. Oram[e], M.J. Oreglia[9], S. Orito[24], J.P. Pansart[21], B. Panzer-Steindel[8], P. Paschievici[26], G.N. Patrick[20], S.J. Pawley[16], P. Pfister[10], J.E. Pilcher[9], J.L. Pinfold[26], D.E. Plane[8], P. Poffenberger[a], B. Poli[2], A. Pouladdej[6], E. Prebys[8], T.W. Pritchard[13], H. Przysiezniak[18], G. Quast[8], M.W. Redmond[9], D.L. Rees[1], K. Riles[4], S.A. Robins[13], D. Robinson[8], A. Rollnik[3], J.M. Roney[9], S. Rossberg[10], A.M. Rossi[2,f], P. Routenburg[6], K. Runge[10], O. Runolfsson[8], D.R. Rust[12], S. Sanghera[6], M. Sasaki[24], A.D. Schaile[10], O. Schaile[10], W. Schappert[6], P. Scharff-Hansen[8], P. Schenk[a], H. von der Schmitt[11], S. Schreiber[3], J. Schwarz[10], W.G. Scott[20], M. Settles[12], B.C. Shen[4], P. Sherwood[15], R. Shypit[b], A. Simon[3], P. Singh[13], G.P. Siroli[2], A. Skuja[17], A.M. Smith[8], T.J. Smith[8], G.A. Snow[17], R. Sobie[g], R.W. Springer[17], M. Sproston[20], K. Stephens[16], H.E. Stier[10], D. Strom[9], H. Takeda[24], T. Takeshita[24], P. Taras[18], S. Tarem[26], P. Teixeira-Dias[11], N.J. Thackray[1], T. Tsukamoto[24], M.F. Turner[5], G. Tysarczyk-Niemeyer[11], D. Van den plas[18], R. Van Kooten[8], G.J. VanDalen[4], G. Vasseur[21], C.J. Virtue[19], A. Wagner[11], C. Wahl[10], J.P. Walker[1], C.P. Ward[5], D.R. Ward[5], P.M. Watkins[1], A.T. Watson[1], N.K. Watson[8], M. Weber[11], S. Weisz[8], P.S. Wells[8], N. Wermes[11], M. Weymann[8], M.A. Whalley[1], G.W. Wilson[21], J.A. Wilson[1], I. Wingerter[8], V-H. Winterer[10], N.C. Wood[16], S. Wotton[8], T.R. Wyatt[16], R. Yaari[26], Y. Yang[4,h], G. Yekutieli[26], I. Zacharov[8], W. Zeuner[8], G.T. Zorn[17].

[1]School of Physics and Space Research, University of Birmingham, Birmingham, B15 2TT, UK
[2]Dipartimento di Fisica dell' Università di Bologna and INFN, Bologna, 40126, Italy
[3]Physikalisches Institut, Universität Bonn, D-5300 Bonn 1, FRG
[4]Department of Physics, University of California, Riverside, CA 92521 USA
[5]Cavendish Laboratory, Cambridge, CB3 0HE, UK
[6]Carleton University, Dept of Physics, Colonel By Drive, Ottawa, Ontario K1S 5B6, Canada
[7]Centre for Research in Particle Physics, Carleton University, Ottawa, Ontario K1S 5B6, Canada
[8]CERN, European Organisation for Particle Physics, 1211 Geneva 23, Switzerland
[9]Enrico Fermi Institute and Department of Physics, University of Chicago,

Chicago Illinois 60637, USA
[10]Fakultät für Physik, Albert Ludwigs Universität, D-7800 Freiburg, FRG
[11]Physikalisches Institut, Universität Heidelberg, Heidelberg, FRG
[12]Indiana University, Dept of Physics, Swain Hall West 117, Bloomington, Indiana 47405, USA
[13]Queen Mary and Westfield College, University of London, London, E1 4NS, UK
[14]Birkbeck College, London, WC1E 7HV, UK
[15]University College London, London, WC1E 6BT, UK
[16]Department of Physics, Schuster Laboratory, The University, Manchester, M13 9PL, UK
[17]Department of Physics and Astronomy, University of Maryland, College Park, Maryland 20742, USA
[18]Laboratoire de Physique Nucléaire, Université de Montréal, Montréal, Quebec, H3C 3J7, Canada
[19]National Research Council of Canada, Herzberg Institute of Astrophysics, Ottawa, Ontario K1A 0R6, Canada
[20]Rutherford Appleton Laboratory, Chilton, Didcot, Oxfordshire, OX11 0QX, UK
[21]DPhPE, CEN Saclay, F-91191 Gif-sur-Yvette, France
[22]Department of Physics, Technion-Israel Institute of Technology, Haifa 32000, Israel
[23]Department of Physics and Astronomy, Tel Aviv University, Tel Aviv 69978, Israel
[24]International Centre for Elementary Particle Physics and Dept of Physics, University of Tokyo, Tokyo 113, and Kobe University, Kobe 657, Japan
[25]Brunel University, Uxbridge, Middlesex, UB8 3PH UK
[26]Nuclear Physics Department, Weizmann Institute of Science, Rehovot, 76100, Israel

[a]University of Victoria, Dept of Physics, P O Box 3055, Victoria BC V8W 3P6, Canada
[b]University of British Columbia, Dept of Physics, 6224 Agriculture Road, Vancouver BC V6T 1Z1, Canada
[c]Also at TRIUMF, Vancouver, Canada V6T 2A3
[d]On leave from Birmingham University, Birmingham B15 2TT, UK
[e]Univ of Victoria, Dept of Physics, P.O. Box 1700, Victoria BC V8W 2Y2,

Canada and TRIUMF, Vancouver, Canada V6T 2A3
[f]Present address: Dipartimento di Fisica, Università della Calabria and INFN, 87036 Rende, Italy
[g]University of British Columbia, Dept of Physics, 6224 Agriculture Road, Vancouver BC V6T 2A6, Canada and IPP, McGill University, High Energy Physics Department, 3600 University Str, Montreal, Quebec H3A 2T8, Canada
[h]On leave from Research Institute for Computer Peripherals, Hangzhou, China

1 Introduction

In Quantum Chromodynamics (QCD), gluons carry a larger color charge than quarks and are more likely to radiate through bremsstrahlung. This leads to the expectation that gluon jets have a softer particle energy spectrum, a larger angular width and a larger particle multiplicity than quark jets with the same energy [1, 2]. For asymptotic energies ($s \to \infty$) and at leading order, QCD predicts a factor 9/4 larger multiplicity for gluon jets than for quark jets [1], for example; the available higher order corrections change this result by only about 10% [3]. For these differences to be visible, it is necessary to relate the QCD predictions directly to the hadron level distributions observed by experiment: it is possible that the confinement of quarks and gluons inside hadrons (fragmentation) or other effects could alter the results from the naive QCD expectation.

A number of experimental searches for differences between quark and gluon jets has been presented [4]. Previous studies in e^+e^- annihilations employed quark and gluon jets with different energies or for which the quark and gluon jets were embedded in different event environments: gluon jets from 3-jet quark-antiquark-gluon $q\bar{q}g$ events at one c.m. energy were compared to quark jets from 2-jet $q\bar{q}$ events at a lower c.m. energy. The quark jet properties for the latter sample were often obtained through interpolation between different data sets instead of from direct measurement. In addition, since the properties of a quark or gluon jet in one event environment are not necessarily the same as those of a quark or gluon jet of equal energy in another environment [5], the interpretation of quark-gluon differences in these studies is not completely straightforward. Use of quark and gluon jets with different energies or environments meant that QCD Monte Carlo calculations were essential to interpret the results. In some cases conflicting results were reported by different experiments. In proton collisions, studies of quark-gluon jet differences have relied on comparison to e^+e^- data, on QCD models or on knowledge of the proton structure functions: again these suffer from indirectness and use of quark and gluon jets with different energies or environments. The evidence obtained for differences between quark and gluon jet properties has therefore been, to date, largely indirect or inconclusive.

In this letter we present a study of quark-gluon jet differences by the OPAL Collaboration at the CERN e^+e^- collider LEP, based on a comparison of quark and gluon jets with essentially the same energy and event environment. The selection of quark and gluon jets with these symmetric properties is possible because quark tagging is employed in 3-jet events, using leptons from the weak decays of charm and bottom quarks. The symmetry between the quark and gluon jets in our study allows a direct comparison of their properties using simple distributions, without reliance on QCD Monte Carlo programs. We demonstrate that our results are not significantly affected by the lepton tag requirement for the quark jet, using a technique which employs data alone. We in addition explicitly separate phenomena related to the regions between jets, such as the so called string effect [6], from this study of the jet peaks themselves, thereby eliminating a source of systematic bias which is present for some previous quark-gluon jet difference studies.

2 Data Sample

The OPAL detector [7] and event trigger [8] are discussed in detail elsewhere. The main detector devices are a large volume central tracking chamber, an electromagnetic calorimeter, a hadron calorimeter and muon detection chambers. The particle and 3-jet event selection criteria are the same as those presented in [6] and so will not be repeated here: we mention only that our analysis employs charged tracks and deposits of energy in the electromagnetic calorimeter ("clusters") which are not associated with a charged track and that events with 3-jet structure are identified using a modified version of the JADE jet-finding algorithm [9]. In this letter, a "particle" therefore refers to a charged track or unassociated cluster: by using only the unassociated clusters we avoid double counting the energy deposited by charged particles in the electromagnetic calorimeter. Starting from a data sample of about 6.5 pb^{-1}, corresponding to 140,189 multi-hadronic Z^0 decays, we obtain 22,721 3-jet events.

To identify quark and gluon jets in the 3-jet sample, we employ lepton tagging. High energy leptons in e^+e^- annihilations are expected to arise primarily from the weak decays of charm c and bottom b quarks. In e^+e^-

collisions, c and b quarks are produced almost exclusively at the electro-weak vertex or in the case of c also through b decay. Therefore the presence of a high energy lepton in a jet identifies it as being a quark jet with high probability: the radiated gluon jet rarely contains a high energy lepton [10]. Muon (μ) and electron (e) candidates in the multi-hadronic events are identified by associating charged tracks reconstructed in the central tracking chamber with independently reconstructed track segments in the hadron calorimeter and muon chambers (for μ) or with electromagnetic clusters (for e): more details are given in [11] and [6]. In this analysis, μ and e candidates are required to have momentum values larger than 3 and 2 GeV/c, respectively.

We retain events from the 3-jet sample for which a lepton candidate (μ or e) is present in one of the two jets with lower energy. The assignment of a particle to a jet is determined by the jet-finding algorithm. This jet with a lepton is assumed to be a quark jet q. The highest energy jet in the 3-jet event is also assumed to be a quark jet since the radiated gluon jet g does not usually have the highest energy in $e^+e^- \rightarrow q\bar{q}g$ events. The remaining jet is assumed to be the gluon jet. We often refer to an antiquark jet $\bar{q}$ as a "quark jet" because there is no distinction between a quark and an antiquark in our analysis. For about 20% of the sample the highest energy jet contains a lepton in addition to one of the two lower energy jets (double tag). For the approximately 80% of the events which are not double tag, the two jets without leptons are required to differ in energy by more than 8 GeV since if their energies were almost the same there would be little information on which was the quark and which was the gluon jet. In this letter, the jet energy E_{jet} refers to the energy calculated using the angles between the jets[1] unless otherwise stated.

To permit a direct comparison of quark-gluon jet properties, the gluon jet in the 3-jet event is required to have the same energy and event environment as the lower energy quark jet: it is these two jets whose properties will be compared. We thus select events from the lepton tagged 3-jet sample for which the angle in the event plane $\psi_{q\bar{q}}$ between the quark and antiquark jets is approximately the same as the angle ψ_{qg} between the high energy quark jet

[1] If the 3 angles between jets in a 3-jet event are labeled ψ_A, ψ_B and ψ_C, then the energy E_α of the jet opposite ψ_α, assuming massless kinematics, is $E_\alpha = E_{c.m.} \cdot sin\psi_\alpha/(sin\psi_A + sin\psi_B + sin\psi_C)$, where $\alpha = A$, B or C.

and the gluon jet. The event plane is defined by the two eigenvectors of the momentum tensor [12] associated with its two largest eigenvalues. We choose $\psi_{q\bar{q}}$ and ψ_{qg} to be $150 \pm 10°$ because this yields a sample with relatively large statistics and high purity values for the quark and gluon jet identification compared to other choices. The gluon and lepton tagged quark jets have energies of about 24.5 GeV for this configuration: we require their energies to be in the range from 20 to 30 GeV in order to further restrict their energies to be the same. In total 155 events are found in this symmetric configuration. The mean jet energy values are 42.6, 24.7 and 24.2 GeV for the higher energy quark jet, the lower energy quark jet and the gluon jet, respectively, with RMS widths of 1.1, 2.4 and 2.2 GeV. The 2% difference between the mean calculated energy values of the gluon and lower energy quark jets is not expected to have a significant impact on the properties of jets studied here. The estimated identification purities are $98 \pm 1\%$, $79 \pm 3\%$ and $77 \pm 3\%$. These jet purity values are obtained using QCD model calculations and full simulation of the detector, as described in [6]. They are given here purely for information and are not used in the data analysis. The main background is from hadrons which are misidentified as leptons or leptons from the decay of light quark hadrons.

Lepton tagging of jets yields a quark jet sample which is atypical, because of the preference for semi-leptonic decays of c and b quarks. To obtain a quark jet sample without these biases, we perform a second selection of data starting with the full 3-jet sample of 22,721 events, using the same selection criteria as are applied to the lepton tagged data but without requiring that a lepton be present. The energy difference between the highest energy jet and a randomly chosen lower energy jet is required to exceed 8 GeV, in analogy with the jet energy difference cut applied to the lepton tagged data.[2] In total 2,189 events are found for which the angle in the event plane between the highest energy jet and each of the two lower energy jets is $150 \pm 10°$ and for which the two lower energy jets have energies in the range from 20 to 30 GeV. The highest energy jet in this second sample is again assumed to be a quark jet, with an estimated purity of $96.4 \pm 0.4\%$, but it is not known which of the two lower energy jets is a quark and which is a gluon jet. Assuming the flavor

[2]This cut is not important since the energy difference between the highest energy and the other two jets is 18 GeV for the events in our study.

independence of the strong coupling constant, it may be presumed that these events represent a normal mixture of quark flavors and hadron decays at the Z^0 peak. In the following, this sample is referred to as the "normal mixture" sample. It is used in conjunction with the lepton tagged sample to obtain quark jet properties which are unaffected by the lepton tagging criteria, as explained in the next section.

3 Observation of Quark-Gluon Jet Differences

3.1 Particle Energy Spectra

We begin the comparison of quark and gluon jets by examining their particle energy spectra. Figure 1 shows the average energy value dE/dn of particles versus the azimuthal angle ψ in the 3-jet event plane, for the lepton tagged and normal mixture data. This distribution is constructed by weighting each particle with its energy value before entering it at its position ψ, which is the angle in the event plane between the particle and the highest energy jet direction. The direction of the highest energy jet is obtained from the jet-finding algorithm. Each bin is normalized by its number of entries dn after all events have been included. The energy values of charged particles are obtained assuming that each has the mass of a charged pion; unassociated electromagnetic clusters are assumed to be photons.

The open points and the histogram in figure 1 (a) show dE/dn versus ψ for the lepton tagged data. The open points show the distribution starting at the higher energy quark jet axis $\psi \equiv 0°$, then proceeding through the lower energy quark jet at $\psi \approx 150°$ to stop halfway around the event plane at $\psi = 180°$. The histogram shows the distribution, again starting at the higher energy quark jet, for the other side of the events: the gluon jet therefore also appears at $\psi \approx 150°$. The region from 112.5° to 180° in ψ is taken to define the jet peaks: this region is delineated by the vertical dashed line in figure 1 (a) and is henceforth called the "jet peak" interval. This interval is chosen so that it is exclusive of that used to study the region *between* jets,

presented in [6]. We also define a "jet core" interval, from 135° to 165° in ψ, which is shown by the dotted lines in figure 1 (a). Summing the particle energies in the jet peak interval for the quark and gluon jets separately, to define a visible jet energy which is independent of the jet-finder, we find the ratio of the mean visible energy of the quark to the gluon jets to be 1.04, in agreement with the result presented for the calculated jet energies in section 2.

Figure 1 (b) shows dE/dn versus ψ for the normal mixture data sample: the solid points show the distribution for randomly chosen halves of the events; the other event halves are shown by the histogram. Each of these curves therefore represents a mixture of 50% gluon and 50% quark jets.

To extract a spectrum for quark jets which is unaffected by the lepton tagging, we employ the following technique which uses OPAL data only. The two distributions of figure 1 (b) – that shown by the histogram and that shown by the solid points – are added together. This gives $[\,dE/dn\,]^{q_n+g_n}$, where q_n and g_n refer to quark and gluon jets from the normal mixture data. We subtract from this sum the distribution $[\,dE/dn\,]^{g_l}$ from the gluon jet side of the lepton tagged events, denoted g_l, shown by the histogram in figure 1 (a). This subtraction is performed bin-by-bin. Assuming the gluon jet properties to be the same in the lepton tagged and normal mixture samples, i.e. $g_l = g_n$, which is a reasonable supposition[3] since the particle and jet selection criteria are the same for the gluon jets in the two samples, this subtraction yields

$$\begin{aligned}[\,dE/dn\,]_i^{q_n+g_n} - [\,dE/dn\,]_i^{g_l} &= [\,dE/dn\,]_i^{q_n} + \{\,[\,dE/dn\,]_i^{g_n} - [\,dE/dn\,]_i^{g_l}\,\} \\ &= [\,dE/dn\,]_i^{q_n} \qquad (1)\end{aligned}$$

where i labels the bin. Thus equation (1) represents a method to obtain quark jet properties "q_n" for a normal mixture of flavors and hadron decays: the extracted distribution $[\,dE/dn\,]^{q_n}$ is shown by the solid points in figure 1 (a). Since the lepton tagged quark jet data, shown by the open points in figure 1 (a), are not used in this procedure, the extracted quark jet distribution is not expected to be biased by the lepton tagging criteria. This same comment holds for the other quark jet measurements presented in this letter,

[3]The correctness of this supposition is supported by Monte Carlo study.

which make use of the extraction technique of equation (1): we refer to these extracted measurements as the "normal mixture quark jet" measurements. The 20% misidentification probability for the gluon jet g_l leads to an equal misidentification probability for these normal mixture quark jets.

From figure 1 (a) it is seen that the mean particle energy for gluon jets (histogram) is smaller than it is for quark jets, in the jet core, regardless of whether the lepton tagged or normal mixture quark jet data (open or solid points) are considered. To further examine this difference, we show in figure 2 (a) the inclusive scaled energy spectrum $(1/n_{total})\, dn/dx_E$ for particles from the jet cores, indicated by open points for the lepton tagged quark jets, by solid points for the normal mixture quark jets and by the histogram for the gluon jets: $x_E = E/E_{jet}$ is the energy of a particle divided by the energy of the jet to which it is assigned by the jet-finder. The normalization is such that the integral of each distribution is unity. The normal mixture quark jet spectrum is obtained using the bin-by-bin technique described above, with dE/dn in equation (1) replaced by $(1/n_{total})\, dn/dx_E$. An overall multiplicative correction of less than 0.1% is applied to the normal mixture quark jet data to bring their integrated area to unity. The softness of the gluon jet spectrum relative to the quark jet one, in the jet core, is apparent from figure 2 (a). This is further illustrated in figure 2 (b) which shows the ratio of $(1/n_{total})\, dn/dx_E$ from the gluon to the normal mixture quark jet. We therefore observe that gluon jets yield a softer particle energy spectrum than quark jets, in the core regions. In contrast, in the jet tails, defined by $112.5° < \psi < 135°$ and $165° < \psi < 180°$ in figure 1 (a), it is seen that the mean particle energy for quark and gluon jets is about the same.

3.2 Particle Multiplicity

Particle multiplicity is independent of the energy spectra examined in section 3.1 because these latter distributions were normalized by the number of particle entries. The inclusive multiplicity distribution versus ψ, or $(1/N_{event})\, dn/d\psi$, is shown in figure 3 (a) for the 3-jet events of our study. These data are plotted like those of figure 1 (a). The histogram for $\psi \approx 150°$ shows the gluon jets; the open points for $\psi \approx 150°$ show the lepton tagged

quark jets. The solid points show the distribution which is obtained using the bin-by-bin subtraction technique of equation (1). Therefore the solid points for $\psi \approx 150°$ show the normal mixture quark jet data. Comparing the normal mixture quark jet distribution to the gluon one, it is seen that they differ in shape: gluon jets have a smaller relative multiplicity in the jet cores and a larger one in the tails. This is better illustrated in figure 3 (b) which shows the ratio of $(1/N_{event})\, dn/d\psi$ from the gluon to the normal mixture quark data, in the jet peak region: we therefore observe that gluon jets are broader than quark jets. This broadness of the gluon jets relative to the quark jets is also apparent in comparison to the lepton tagged quark jet data in figure 3 (a): thus the same qualitative difference between quark and gluon jet structure is observed regardless of which of the two quark jet samples is considered. This is analogous to what was found for the energy spectra presented in section 3.1.

The mean particle multiplicity value $< n >$ of the jets is obtained by integrating the distributions in figure 3 (a) over the jet peak regions. For the normal mixture quark jets, we find $< n >_{quark} = 12.5 \pm 0.3$ and $< n_{ch} >_{quark} = 7.2 \pm 0.2$ for the total and charged mean multiplicities. The lepton tagged quark jets yield 10.9 ± 0.3 and 6.8 ± 0.2, which are 13% and 6% smaller. These values are not corrected for the effects of detector acceptance and resolution, selection cuts and quark-gluon jet misidentification. The errors are statistical only. The difference between the mean multiplicity values of the normal mixture and lepton tagged quark jets is explained by their different composition of quark flavors and hadron decays, as has been checked through Monte Carlo calculation. For the gluon jets we find $< n >_{gluon} = 12.9 \pm 0.3$ and $< n_{ch} >_{gluon} = 7.4 \pm 0.2$. The ratio of mean multiplicity from the gluon to the normal mixture quark jets is therefore

$$\frac{< n >_{gluon}}{< n >_{quark}} = 1.03 \pm 0.03 \, ^{+0.15}_{-0.00} \qquad (2)$$

$$\frac{< n_{ch} >_{gluon}}{< n_{ch} >_{quark}} = 1.02 \pm 0.04 \, ^{+0.06}_{-0.00}$$

where the first error is statistical and the second is systematic. The systematic error is defined by the difference between the result obtained from the normal mixture and lepton tagged quark jet data: this conservatively treats the entire difference as an error. We therefore observe little difference

between the mean multiplicity values of quark and gluon jets. The similarity in these multiplicity values is consistent with the essentially equal energies of the quark and gluon jets because their mean particle energy values, integrated over the entire jet peak, are also quite similar: the softness of the gluon jet particle energy spectrum relative to the quark jet one is present only in the jet core, as discussed in section 3.1.[4] Effects related to detector acceptance, resolution and selection cuts largely cancel in the ratios (2): their overall effect is estimated to be smaller than the statistical errors, as discussed in section 4, and so no correction is applied for them.

It is interesting that the difference between the open and solid points in figure 3 (a) is small in the region between jets, i.e. for $37.5° < \psi < 112.5°$. This is more clearly visible in figure 3 (c) which shows the same data on a logarithmic scale. Thus the principal difference between quark jets in the lepton tagged and normal mixture samples appears in the peaks, as would be naively expected. This is in agreement with the conclusions of [6], in which an explicit study of the multiplicity distribution in the region between jets is presented. Here a different method for estimating the effect of lepton tagging which relies entirely on OPAL data is employed, further establishing the results of [6] and in particular its model independent nature.

3.3 Particle p_{in} and p_{out} Distributions

We next examine the inclusive distributions of particle momentum p_{in} and p_{out}, in and out of the 3-jet event plane, versus the azimuthal angle ψ. These distributions combine energy and multiplicity information and so, taken together, are not independent of the distributions discussed in the previous sections. Resolved into its orthogonal components, particle momentum yields additional, detailed information about quark and gluon jet structure, however.

Figures 4 (a) and (b) show $(1/N_{event})\, dp_{in}/d\psi$ and $(1/N_{event})\, dp_{out}/d\psi$.

[4] Integrated over the core region, the mean particle energy values of quark and gluon jets differ by about 12%; this difference is reduced to 7% if the entire jet peak region is included, corresponding to the 3% higher mean multiplicity and 4% smaller mean visible jet energy of the gluon relative to the quark jets.

The meaning of the histogram and points with errors is the same as in figure 1 (a). Comparison of the gluon jets (histogram) to either the lepton tagged or normal mixture quark jets (open or solid points), in the jet peak regions, shows that the gluon jet distribution is wider than the quark jet one for both dimensions. This complements the result found from the shape of the multiplicity distribution in section 3.2. Comparing these p_{in} and p_{out} spectra to the data in figures 1 (a) and 3 (a), it may be deduced that the different shape of quark and gluon jets for the p_{out} component is mostly related to the shape of multiplicity: the mean p_{out} values for quark and gluon jets, as a function of ψ, are about the same. For the p_{in} component, the relative broadness of the gluon jets is related to their softer energy spectrum in the jet core, in addition to their different shape in multiplicity. Figure 4 (c) shows the ratio of $(1/N_{event})\, dp_{in}/d\psi$ from the gluon to the normal mixture quark jet, in the jet peak interval. The analogous ratio for $(1/N_{event})\, dp_{out}/d\psi$ is similar to what is shown to figure 3 (b). A smaller fraction of the gluon jet energy is in the core and a larger fraction is in the tail, emphasizing its broadness relative to the quark jet.

To obtain a quantitative measure of the widths of the quark and gluon jets, we fit the jet peak regions in figures 4 (a) and (b) with Gaussian distributions, which provide good descriptions of these regions. These fits yield standard deviation values of $\sigma_q^{in} = 8.9 \pm 0.4°$ and $\sigma_q^{out} = 11.6 \pm 0.8°$ for the normal mixture quark jets and $\sigma_g^{in} = 12.7 \pm 0.5°$ and $\sigma_g^{out} = 17.0 \pm 1.1°$ for the gluon jets, for the p_{in} and p_{out} components. The ratios of the gluon to the quark jet widths are therefore

$$\frac{\sigma_g^{in}}{\sigma_q^{in}} = 1.42 \pm 0.08\,^{+0.04}_{-0.00} \qquad (3)$$

$$\frac{\sigma_g^{out}}{\sigma_q^{out}} = 1.46 \pm 0.14\,^{+0.06}_{-0.00}$$

where the first error is statistical and the second, systematic error is defined as for the multiplicity ratios (2). As before, these values are not corrected for the effects of detector acceptance and resolution, event selection and quark-gluon jet misidentification. As for multiplicity, we find that the ratios (3) are insensitive to all but this last factor.

4 Comparison with Models

In this section we compare the predictions of QCD Monte Carlo models to data, to see how well they reproduce the observed quark-gluon jet differences. We also use the Monte Carlos to check our method (1) of extracting normal mixture quark jet properties from the data. We choose two models: Jetset [14] version 7.2 and Cojets [15] version 6.12. Both these models have been tuned to provide a good description of the global characteristics of multihadronic events in Z^0 decays: Jetset by OPAL as presented in [16] and Cojets by its author [15], using the data in [16].

The underlying quark-gluon state for Jetset and Cojets is obtained with a parton shower, in which virtual quarks and antiquarks created in the simulated Z^0 decays evolve toward their mass shells through parton emission, as do partons created through the emissions. The mass cutoff which terminates shower evolution is larger in Cojets than it is in Jetset (3 GeV/c^2 versus 1 GeV/c^2): this means that differences between quark and gluon jets at the parton level, related to the different color charges of quarks and gluons, are less important in the former case. For example, there are on average 3.2 partons which are present at the end of the parton shower in Cojets, compared to 9.1 in Jetset, for a normal mixture of hadronic Z^0 events. Thus it is unlikely that a gluon jet in a 3-jet $q\bar{q}g$ Cojets event will evolve to such a degree, through additional gluon bremsstrahlung, that its energy and angular structure will differ much from those of a quark jet: larger parton level differences are expected for Jetset. The two Monte Carlo programs also differ in their mechanism for hadronization. Jetset incorporates the Lund model for fragmentation [17], in which a one-dimensional color flux tube or "string" connects a quark with an antiquark, with gluons as kinks on the string. Since quarks and antiquarks terminate strings while gluons do not, an inherent asymmetry exists between quark and gluon hadronization properties. Cojets incorporates an independent fragmentation model [18], in which partons hadronize in quasi-isolation from each other. With the present parameter values of Cojets, the properties of quark and gluon hadronization are the same. Thus Cojets is not expected to exhibit significant differences between quark and gluon jet structure, in contrast to Jetset.

Figures 5 (a) and (b) show the prediction of Jetset for the mean particle energy distribution dE/dn versus ψ. Full simulation of the OPAL detector [19] is included. The events in figure 5 (a) are selected using the same criteria as are applied to the data, including lepton tagging. The events in figure 5 (b) are selected in the same manner except without lepton tagging: these events contain a normal mixture of quark flavors and hadron decays at the Z^0 peak. The quark and gluon jets in this latter sample are identified perfectly using Monte Carlo information as described in [6]; the jets are then mixed to correspond to the misidentification level present for figure 5 (a) and the data. The histograms and points with errors in figure 5 are defined as in figure 1 (a).

It is seen for the lepton tagged Jetset events in figure 5 (a) that the mean particle energy value from quark jets (points with errors) is larger than that from gluon jets (histogram) in the core region $\psi \approx 150°$, while the quark and gluon jet distributions are about the same in the jet tails. These same features are also present in figure 5 (b) for the normal mixture Jetset events. This agrees with data, cf. figure 1 (a). The dashed and solid histograms in figures 2 (b), 3 (b) and 4 (c) show the predictions of these same lepton tagged and normal mixture Jetset samples, for the ratio of $(1/n_{total})\, dn/dx_E$, $(1/N_{event})\, dn/d\psi$ and $(1/N_{event})\, dp_{in}/d\psi$ from the gluon to the quark jets. Again, the Monte Carlo curves are all in good agreement with the data. Thus Jetset describes the measured quark-gluon jet differences quite well. The qualitative features which differentiate quark and gluon jet structure are present for both the lepton tagged and normal mixture samples. This also agrees with the observations of section 3: here these observations are obtained independently, using the Monte Carlo technique.

For the sample of Jetset events shown in figure 5 (b), with a normal mixture of quark flavors and hadron decays, we obtain $< n >_{gluon} / < n >_{quark} = 1.12 \pm 0.01$ and $< n_{ch} >_{gluon} / < n_{ch} >_{quark} = 1.11 \pm 0.01$, for the ratio of mean multiplicity from the gluon to the quark jets, defined as in section 3.2. At the generator level, that is without detector simulation, including all particles with a lifetime larger than $3 \cdot 10^{-10}$ s and the same level of quark-gluon jet misidentification as is estimated for the data, ratios are derived which agree with these to within the statistical errors. This justifies the statement made in section 3.2 that effects related to detector simulation and selection

cuts cancel in these ratios. The multiplicity ratios from Jetset are somewhat larger than the measured ones (2) but there is overall agreement to within the quoted uncertainties. These same Jetset events yield $\sigma_g^{in}/\sigma_q^{in} = 1.31 \pm 0.02$ and $\sigma_g^{out}/\sigma_q^{out} = 1.29 \pm 0.04$ for the ratios of the gluon to quark jet widths, defined as in section 3.3: in this case the Monte Carlo values are somewhat smaller than the measured ones, given in (3), but again are in basic agreement with them, to within the errors.

Figure 5 (c) shows dE/dn versus ψ for a sample of Cojets events with a normal mixture of quark flavors and hadron decays. The Cojets distribution is constructed at the generator level using the same selection criteria as are applied to the data except for the lepton tagging: the quark and gluon jets are identified using Monte Carlo information and then mixed to correspond to the misidentification level estimated for the data. Simulation of the detector is found to have a small effect on dE/dn: thus this Cojets distribution can be compared directly to the Jetset one in figure 5 (b). The Cojets events do not exhibit a significant difference between quark and gluon jets: in conjunction with the results shown for Jetset this demonstrates the sensitivity of dE/dn versus ψ to differences between quark and gluon jet properties. The same result is found for the other distributions in our study: Cojets predicts essentially no difference between quark and gluon jets – as is expected for the current version – in contrast to Jetset which exhibits differences in qualitative agreement with data as presented above.

5 Discussion and Summary

Lepton tagging of quarks has been used to separate quark and gluon jets in e^+e^- 3-jet events. The highest energy jet in the 3-jet events is assumed to be a quark jet q (or antiquark jet $\bar{q}$). Of the two lower energy jets, one is required to have an electron e or muon μ track candidate. This e or μ is assumed to come from a semi-leptonic charm or bottom quark decay and so identifies the jet as being the other quark (or antiquark) jet. The remaining jet is assumed to be the gluon jet. Use of the lepton to identify the two lower energy jets allows events with a symmetric topology to be studied, in which the angle $\psi_{q\bar{q}}$ between the quark and antiquark jets is the same as the angle

ψ_{qg} between the high energy quark and the gluon jet. Thus our method allows quark and gluon jets with essentially the same energy and event environment to be selected, so that their properties can be compared directly: in previous studies of quark-gluon jet differences the quark and gluon jets had different energies or environments, introducing systematic uncertainty. We choose $\psi_{q\bar{q}} = \psi_{qg} = 150 \pm 10°$, yielding events in which the gluon and lower energy quark jets both have energies of about 24.5 GeV: it is these two jets whose properties are compared. A second sample of 3-jet events is selected, with the same topology as these lepton tagged data but without requiring a lepton tag. By subtracting the gluon jet distribution of the first sample from the sum of the quark and gluon jet distributions of the second sample, we derive quark jet properties which represent a normal mixture of flavors and hadron decays on the Z^0 resonance, free from the effect of the lepton tagging. The two independent quark jet data sets – the lepton tagged and normal mixture one – exhibit the same qualitative differences relative to the gluon jets, when their properties are compared: we thus find that the lepton tag does not affect the qualitative differences observed between quark and gluon jet structure, for the distributions we study. Our analysis is based on data only and so is model independent. Monte Carlo models are used only as an independent check of the results.

From this study, we observe that gluon jets have a softer particle energy spectrum than quark jets in the jet cores, while the energy spectra for the two jet types are similar in the jet tails. We observe, in addition, that gluon jets are broader than quark jets: this is seen both from the shape of the multiplicity distribution and from the shape of the inclusive particle momentum spectra, $(1/N_{event})\, dp_{in}/d\psi$ and $(1/N_{event})\, dp_{out}/d\psi$, in and out of the 3-jet event plane. Measured by the standard deviation values obtained from Gaussian fits to the jet peak regions of $(1/N_{event})\, dp_{in}/d\psi$ and $(1/N_{event})\, dp_{out}/d\psi$, the difference in width is measured to be about 40% for both directions. These values are not corrected for the estimated level of quark-gluon jet misidentification, which is 21% for the quark jet and 23% for the gluon jet. We find little difference, in contrast, between the mean particle multiplicity value $< n >$ for quark and gluon jets. That gluon jets are wider and yield a softer particle energy spectrum than quark jets fits well with the expectations of perturbative QCD. In contrast, the expectation that the ratio of mean particle multiplicity from gluon to quark jets should be about 9/4 is

not supported by our study. This QCD prediction is not directly comparable to our measurement, however, because our analysis is based on quark and gluon jets in $q\bar{q}g$ 3-jet topologies whereas the theoretical prediction of 9/4 is obtained by comparing the final-state parton multiplicity produced by a virtual gluon-gluon gg system to that produced by a virtual quark-antiquark $q\bar{q}$ one, at asymptotic energies.

6 Acknowledgements

We thank Kiusau Tesima for helpful remarks. It is a pleasure to thank the SL Division for the efficient operation of the LEP accelerator and their continuing close cooperation with our experimental group. In addition to the support staff at our own institutions we are pleased to acknowledge the following :

Department of Energy, USA
National Science Foundation, USA
Science and Engineering Research Council, UK
Natural Sciences and Engineering Research Council,Canada
Israeli Ministry of Science
Minerva Gesellschaft
The Japanese Ministry of Education, Science and Culture (the Monbusho) and a grant under the Monbusho International Science Research Program.
American Israeli Bi-national Science Foundation.
Direction des Sciences de la Matière du Commissariat à l'Energie Atomique, France.
The Bundesministerium für Forschung und Technologie, FRG.
and The A.P. Sloan Foundation.

References

[1] S. J. Brodsky and J. Gunion, Phys. Rev. Lett. **37** (1976) 402.

[2] K. Shizuya and S.-H. H. Tye, Phys. Rev. Lett. **41** (1978) 787;
M. B. Einhorn and B. G. Weeks, Nucl. Phys. **B146** (1978) 445.

[3] A. H. Mueller, Nucl. Phys. **B241** (1984) 141;
J. B. Gaffney and A. H. Mueller, Nucl. Phys. **B250** (1985) 109.

[4] JADE Collaboration, W. Bartel *et al.*, Phys. Lett. **123B** (1983) 460;
UA2 Collaboration, P. Bagnaia *et al.*, Phys. Lett. **144B** (1984) 291;
HRS Collaboration, M. Derrick *et al.*, Phys. Lett. **165B** (1985) 449;
MARK2 Collaboration, A. Petersen *et al.*, Phys. Rev. Lett. **55** (1985) 1954;
UA1 Collaboration, G. Arnison *et al.*, Nucl. Phys. **B276** (1986) 253;
TASSO Collaboration, W. Braunschweig *et al.*, Z. Phys. **C45** (1989) 1;
AMY Collaboration, Y. K. Kim *et al.*, Phys. Rev. Lett. **63** (1989) 1772.

[5] See, for example, W. de Boer, CERN-PPE/90-161; Proc. SLAC Summer Institute on Particle Physics, Stanford 1990.

[6] OPAL Collaboration, M. Z. Akrawy *et al.*, CERN-PPE/91-31 (1991).

[7] OPAL Collaboration, K. Ahmet *et al.*, CERN-PPE/90-114 (1990), submitted to Nucl. Instr. and Meth.

[8] M. Arignon *et al.*, CERN-PPE/91-32 (1991), submitted to Nucl. Instr. and Meth.

[9] JADE Collaboration, W. Bartel *et al.*, Z. Phys. **C33** (1986) 23;
OPAL Collaboration, M. Z. Akrawy *et al.*, Z. Phys. **C49** (1991) 375.

[10] See, for example, H. P. Nilles and K. H. Streng, Phys. Rev. **D23** (1981) 1944.

[11] OPAL Collaboration, M. Z. Akrawy *et al.*, CERN-PPE/91-48 (1991).

[12] J. D. Bjorken and S. J. Brodsky, Phys. Rev. **D1** (1970) 1416;
MARK2 Collaboration, G. Hanson *et al.*, Phys. Rev. **D26** (1982) 991.

[13] CLEO Collaboration, M. S. Alam *et al.*, Phys. Rev. Lett. **49** (1982) 357.

[14] T. Sjöstrand, Comp. Phys. Comm. **39** (1986) 347;
T. Sjöstrand and M. Bengtsson, Comp. Phys. Comm. **43** (1987) 367.

[15] R. Odorico, Comp. Phys. Comm. **32** (1984) 139; Comp. Phys. Comm. **59** (1990) 527.

[16] OPAL Collaboration, M. Z. Akrawy *et al.*, Z. Phys. **C47** (1990) 505.

[17] B. Andersson *et al.*, Phys. Rep. **97** (1983) 31.

[18] R. Field and R.P. Feynman, Nucl. Phys. **B136** (1978) 1.

[19] J. Allison *et al.*, Comp. Phys. Comm. **47** (1987) 55;
D. R. Ward, Proc. MC'91 Workshop, NIKHEF, Amsterdam, 1991.

Figure Captions

Figure 1. (a) The mean particle energy dE/dn versus the azimuthal angle ψ in the 3-jet event plane. The open points and histogram show the distribution for the lepton tagged data. For the open points, the distribution starts at the high energy quark jet, then proceeds to the low energy quark jet. The histogram shows the other event halves: from the high energy quark to the gluon jet. The solid points show the equivalent of the open points, for data representing a normal mixture of quark flavors and hadron decays, which are obtained from OPAL measurements as described in the text. (b) dE/dn versus ψ for events with the same geometry as those in (a), without the requirement of a lepton tag. The histogram and solid points show randomly selected halves of the events.

Figure 2. (a) The scaled inclusive energy spectrum $(1/n_{total})\, dn/dx_E$ of particles from the core region of the jets. (b) The ratio of $(1/n_{total})\, dn/dx_E$ from the gluon to the normal mixture quark jet data. Also shown are calculations from the Jetset Monte Carlo, which include detector simulation and the same level of quark-gluon jet misidentification as is estimated for the data.

Figure 3. (a,c) The inclusive multiplicity distribution $(1/N_{event})\, dn/d\psi$. The histogram and points with errors are defined as in figure 1 (a). (b) The ratio of $(1/N_{event})\, dn/d\psi$ from the gluon to the normal mixture quark jets, in the jet peak. The Monte Carlo curves are defined as in figure 2 (b).

Figure 4. The inclusive momentum distribution for (a) the component in the event plane $(1/N_{event})\, dp_{in}/d\psi$ and (b) the component out of the event plane $(1/N_{event})\, dp_{out}/d\psi$. The histogram and points with errors are defined as in figure 1 (a). In the first, off-scale bin of (a), the 3 curves each have a value of about 1.85. (c) The ratio of $(1/N_{event})\, dp_{in}/d\psi$ from the gluon to the normal mixture quark jets, in the jet peak. The Monte Carlo curves are defined as in figure 2 (b).

Figure 5. dE/dn versus ψ for the Jetset and Cojets Monte Carlos. The distributions are constructed as in figure 1 (a). Simulation of the detector is included for (a) and (b). Quark and gluon jets are separated using lepton tagging for (a) and Monte Carlo information for (b) and (c). All the Monte Carlo samples include the same level of quark-gluon jet misidentification as is estimated for the data.

Figure 1

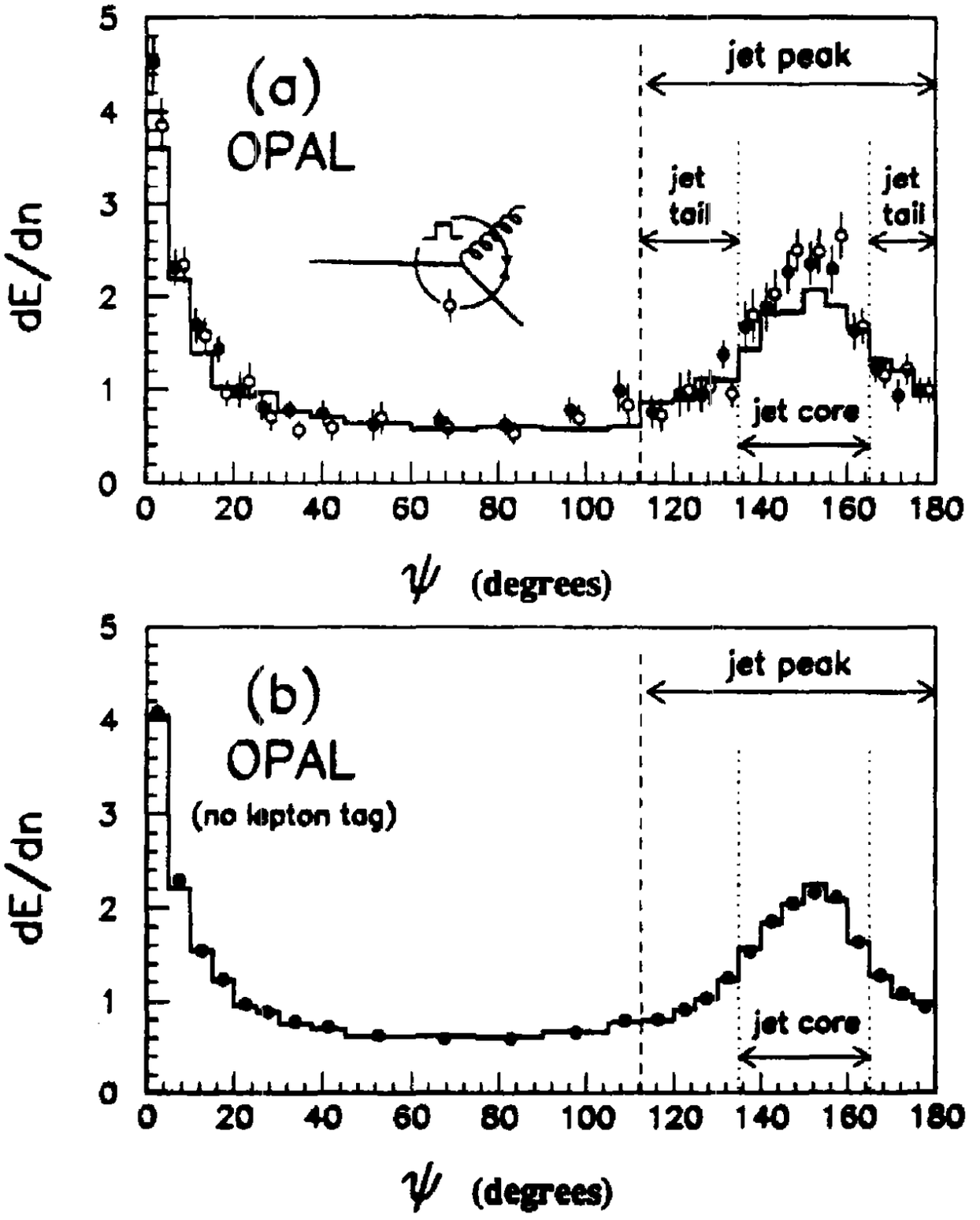
(a)
OPAL
jet peak
jet tail
jet tail
jet core
dE/dn
ψ (degrees)
(b)
OPAL
(no lepton tag)
jet peak
jet core
dE/dn
ψ (degrees)

Figure 2

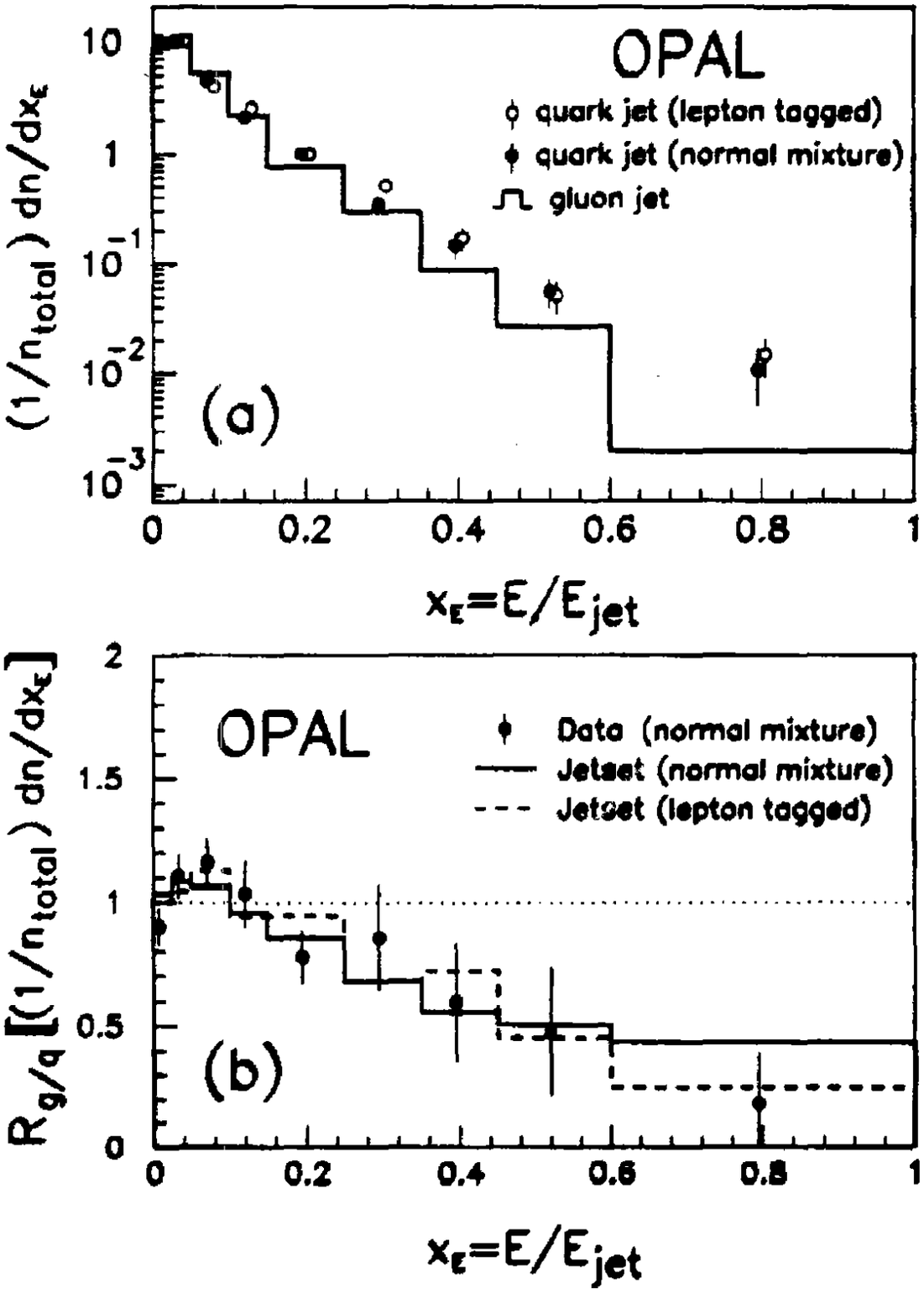
OPAL
quark jet (lepton tagged)
quark jet (normal mixture)
gluon jet
(a)
$(1/n_{total})\, dn/dx_E$
$x_E = E/E_{jet}$
OPAL
Data (normal mixture)
Jetset (normal mixture)
Jetset (lepton tagged)
(b)
$R_{g/q}\,[(1/n_{total})\, dn/dx_E]$
$x_E = E/E_{jet}$

Figure 3

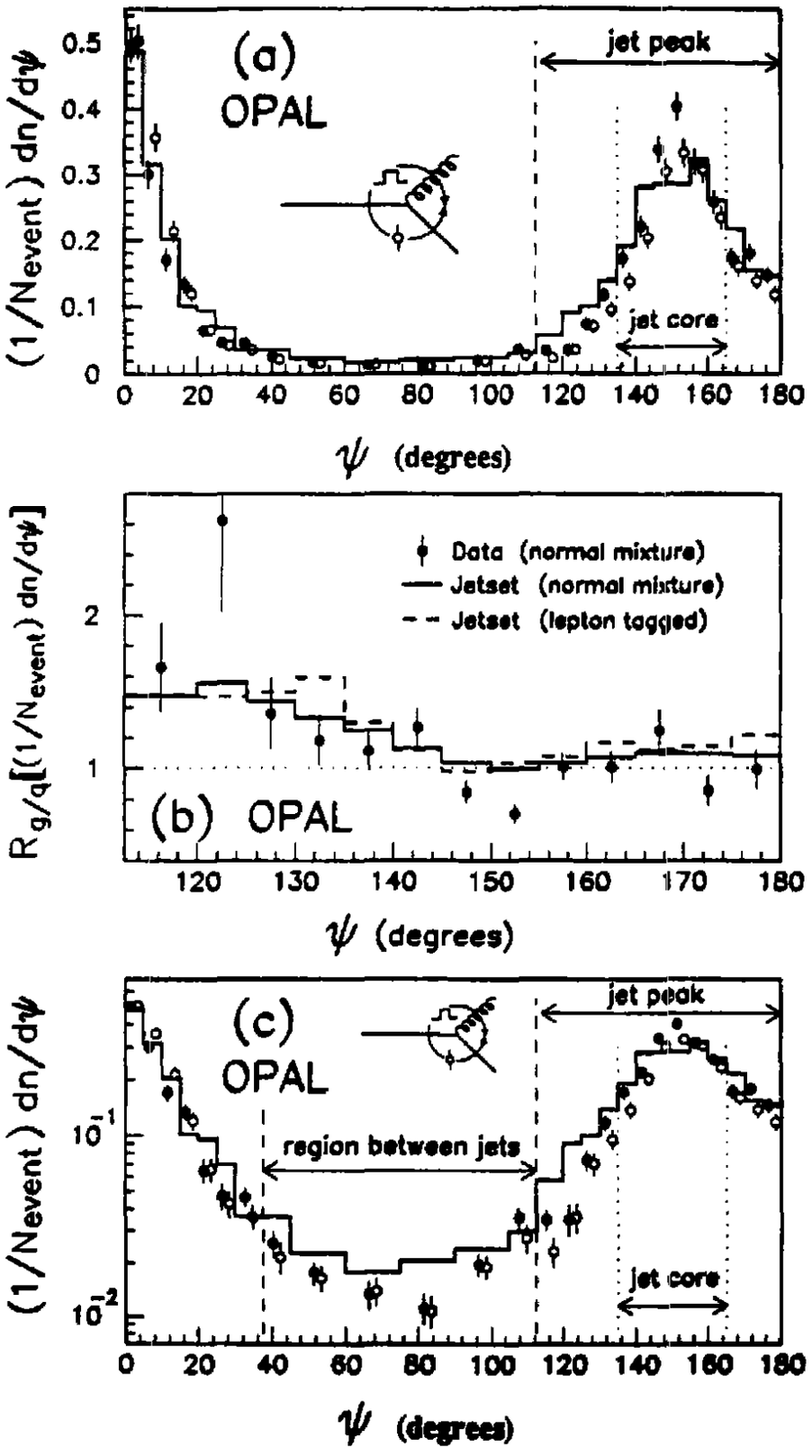
(a)
OPAL
jet peak
jet core
(1/Nevent) dn/dψ
ψ (degrees)
Data (normal mixture)
Jetset (normal mixture)
Jetset (lepton tagged)
(b) OPAL
Rg/q[(1/Nevent) dn/dψ]
ψ (degrees)
(c)
OPAL
jet peak
region between jets
jet core
(1/Nevent) dn/dψ
ψ (degrees)

Figure 4

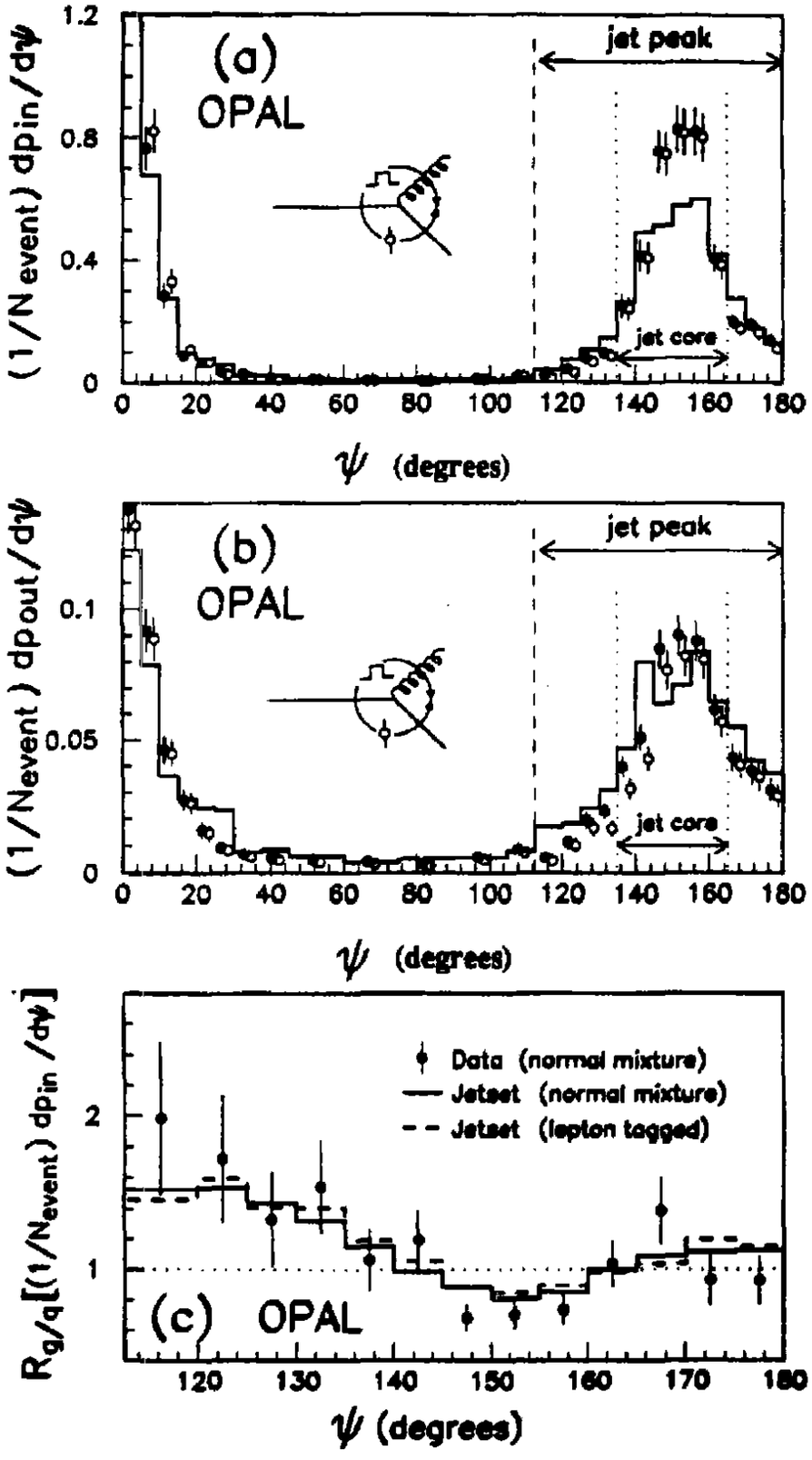
(a)
OPAL
jet peak
jet core
(1/N event) dpin/dψ
ψ (degrees)
(b)
OPAL
jet peak
jet core
(1/Nevent) dpout/dψ
ψ (degrees)
Data (normal mixture)
Jetset (normal mixture)
Jetset (lepton tagged)
(c) OPAL
Rg/q[(1/Nevent) dpin /dψ]
ψ (degrees)

Figure 5

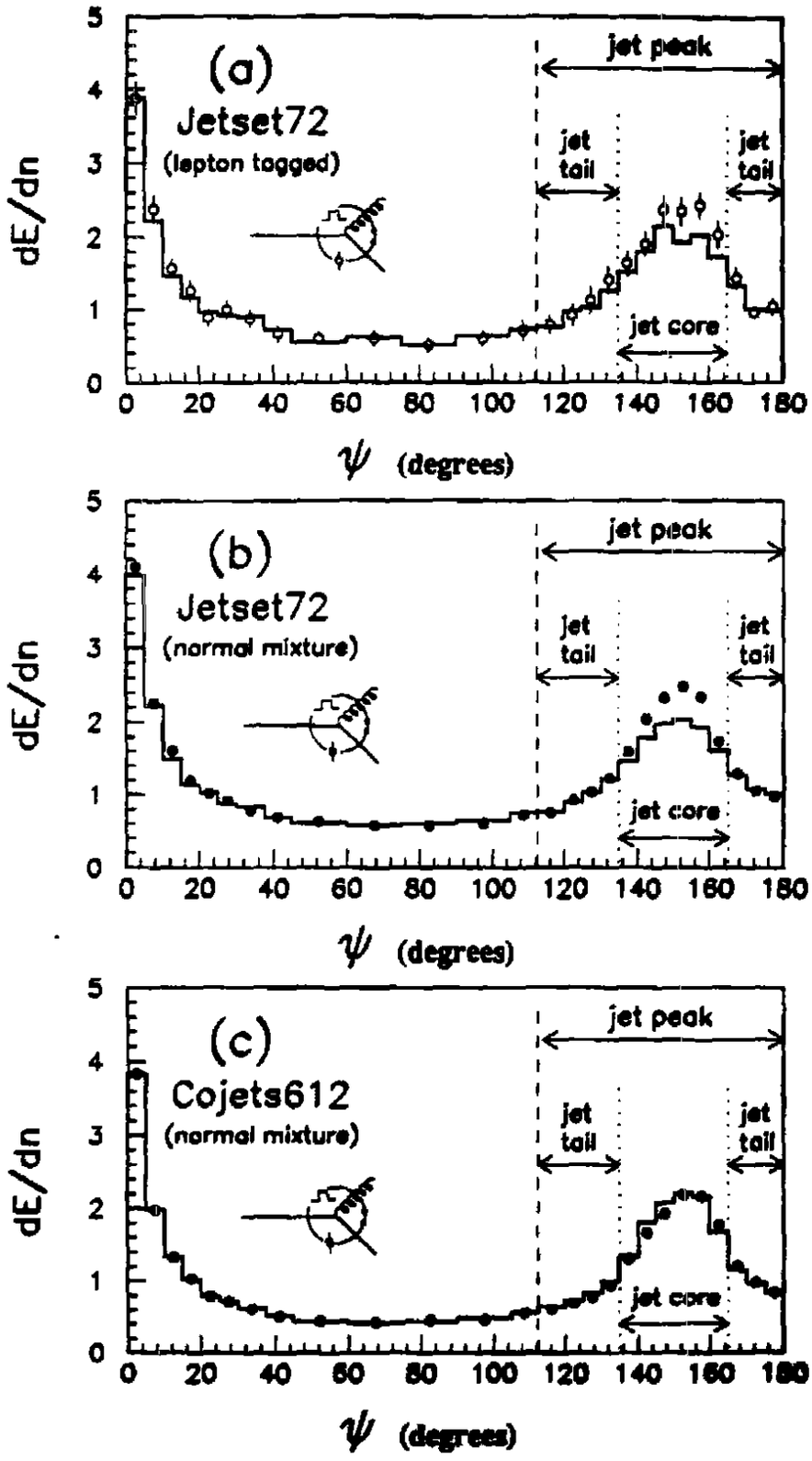
(a)
Jetset72
(lepton tagged)
jet peak
jet tail
jet tail
jet core
dE/dn
ψ (degrees)
(b)
Jetset72
(normal mixture)
jet peak
jet tail
jet tail
jet core
dE/dn
ψ (degrees)
(c)
Cojets612
(normal mixture)
jet peak
jet tail
jet tail
jet core
dE/dn
ψ (degrees)